PAPER

Check for updates

Rayleigh anomaly induced phase gradients in finite nanoparticle chains†

Lior Michaeli, [iD] *‡[a,b,c] Ofer Doron,[a,b,c] Yakir Hadad,[a] Haim Suchowski[b,c] and Tal Ellenbogen[a,c]

Collective optical interactions in infinite nanoparticle arrays have been studied intensively over the past decade. However, analysis of finite arrays has received significantly less attention. Here, we theoretically and numerically show that the collective interaction in finite nanoparticle chains can support phase gradients that shift the diffraction pattern with respect to infinite chains. Specifically, we demonstrate that this phenomenon occurs for resonating nanoparticles in a narrow spectral range around the Rayleigh anomaly condition, *i.e.*, when a certain diffraction order radiates at a grazing angle. This reveals that the Rayleigh anomaly, which is associated with intensity changes, can also induce angular anomalies in finite arrays. To study the effect theoretically, we develop a novel analytical approach based on the discrete dipole approximation. Within this framework, we find an approximate closed-form solution to the particles' dipole moments. We show that our solution can be expressed in two different ways, one based on a combinatorial calculation, and the other on a recursive calculation, and discuss the unique physical interpretation emerging from each of them. Our results are of potential importance in a wide range of practical applications from LIDARs to beam shaping schemes.

I. Introduction

The interaction between light and nanostructured periodic systems has been at the focus of extensive research over the past two decades. A central topic of ongoing interest in the field deals with the collective response of periodic systems and its influence on the interaction with light.[1–3] It was shown that collectivity of the system may significantly enhance light–matter interaction and support a plethora of attractive and highly tailorable physical phenomena.[1–3] For example, it can

[a]*Department of Physical Electronics, Faculty of Engineering, Tel-Aviv University, Tel-Aviv 6779801, Israel. E-mail: liormic1@caltech.edu*
[b]*Raymond and Beverly Sackler School of Physics & Astronomy, Tel-Aviv University, Tel-Aviv 6779801, Israel*
[c]*Center for Light-Matter Interaction, Tel-Aviv University, Tel-Aviv 6779801, Israel*
†Electronic supplementary information (ESI) available: Derivation of an analytical condition for the model accuracy. Numerical verification of the model accuracy. Number of scattering paths as a function of the number of particles in the chain. An example of a nanoparticle the supports the studied polarizability. Studied wavelength dependent polarizability. Diffraction patterns of the studied chain. The effect of RA induced phase gradients in longer chains. Understanding the phase gradients from the dependence of B_q on q. RA induced transparency analysis by the developed framework. Analysis of RA induced phase gradients with an established macroscopic theory. Calculation of the power of the diffracted beams. Persistence of the angular deviation with varying degree of the radiative loss rate. See DOI: https://doi.org/10.1039/d3nr02293e
‡Currently at: Thomas J. Watson Laboratories of Applied Physics, California Institute of Technology, Pasadena, California, 91125, USA.

be beneficial for nonlinearity enhancement and manipulations,[4–8] induced transparency and slow light windows,[9–11] sensing,[12–15] lasing[16–19] and even for stimulating Bose–Einstein condensation at room temperature.[20]

The theoretical analysis of periodic nanostructured systems usually requires the use of approximations that hide the full dynamics. In the simplistic case of an infinite array illuminated by a plane wave, all the nanoparticles are imposed with equal dipole moment amplitudes, and phase profiles dictated by the angle of incident light, according to Bloch's theorem. However, for finite arrays, the solution is not restricted and the interaction between the nanoparticles can induce a spatial distribution of the dipole moment values over the array. The variety of phenomena emerging from this spatial distribution have been explored extensively in the microwave regime,[21,22] and more recently received some attention also in the optical regime.[18,23–31] These dipole moment variations across the array may influence the radiation to the far-field, for example, by causing a change in the diffracted beam width and shape or stimulating the radiation of leaky waves. Notably, in these examples, the directions of reflection and diffraction of the array still follow the grating equation for infinite arrays. The modified far-field radiation may reveal intriguing physical properties of the studied devices. For example, lately, it has been shown that *via* far-field analysis of leaky-waves radiation, the topological properties and invariants of periodic arrays can be probed.[32,33] In the context of collective modes supported by

the array, *i.e.*, in vicinity to the Rayleigh anomaly (RA) condition, several works have also studied the evolution of the spectral response and associated quality factor as a function of the array size.[34–39] The dynamics in finite nanoparticle arrays are often explained by the modal solutions of the infinite array.[25,26,40,41] While this approach is elegant and compact in the sense that it uses a few global wave functions that encapsulate the microscale interactions, the echoing multi-scattering processes that build up the modes are hidden in such analysis.

Here, we use a microscopic approach to explore the effect of the multi-scattering process in finite chains on the spatial distribution of the nanoparticles' excitation. This approach provides a new physical picture of the interaction and allows us to reveal new associated dynamics. Particularly, while the famous RA condition is associated with intensity anomalies of the light for over a century, we hereby show how non-trivial *phase anomalies* can emerge at that condition. In turn, these lead to an interesting outcome, an *angular diffraction anomaly*, whereby the diffraction directions from finite chains deviate from the universally known grating equation. In addition, we show that the chain's multi-scattering process can be described by recursive relations dictated by the generalized form of the Fibonacci series, a ubiquitous feature of nature. An alternative explicit solution based on the multinomial coefficient is presented, which reveals the combinatorial nature of the underlying dynamics. We use the developed model to explore the buildup of the studied mode and show how the scattering paths interference becomes interesting and non-trivial as the comprising particles become resonant. Finally, we link the newly developed theory of the microscopic picture and the well-established theory of the macroscopic picture.

The paper is organized as follows: in Section II we first present the theory of the discrete dipole approximation (DDA) and then introduce the solution for infinite chains (Section II-A). Next, we derive the model for finite chains (Section II-B) and then introduce two different analytical solutions for the chain excitation (Sections II-C and II-D). In Section III, we demonstrate the novel phenomenon of RA induced phase gradients and use the developed model to explore its origin. In Section IV we show how the phase gradients cause angular reflection and diffraction anomalies. In Section V, we use the model to analyze the chain dynamics by multiple scattering path interference. In Section VI we show how the explored phenomena can also be interpreted according to an existing theory for the macroscopic dynamics of the chain. Conclusions and outlook are given in Section VII.

II. Theory

To analyze the spatial profile of the chain's excitation under plane wave illumination, we use the DDA.[42,43] This model serves to find the dipole moments' vector p_i of each of the N nanoparticles composing an array of arbitrary geometry ($i = 1, ..., N$) by solving a system of $3N$ coupled equations, which accounts for the mutual influence of all nanoparticles. To obtain physical insight, we will consider the simplified case of a finite 1D chain of N identical, equally spaced nanoparticles. In addition, for simplicity, we will derive the model within the scalar approximation, where a specific polarization component governs the interaction. We denote the polarizability of the particle located at r_i, by $\alpha_{s,i}$, and express the dipole moments at the ith location as:

$$p_i = p(r_i) = \alpha_{s,i}E_{loc,i} \tag{1}$$

where $E_{loc,i} = E_{loc}(r_i)$ is the local electric field at r_i, and stands for the field at the particle's location but in the absence of the particle itself. This field is composed of the applied field, denoted as $E_{app,i}$, and the retarded scattered fields from all other particles $E_{sca,i}$, at that location:

$$E_{loc,i} = E_{app,i} + E_{sca,i} = E_{app,i} + \sum_{j \neq i} G_{ij}p_j \tag{2}$$

where G_{ij} ($= G(|r_i - r_j|)$) is the electric dipole Green function that describes the interaction between the ith and j^{th} dipoles:[44]

$$G_q = g_q e^{ikr_q}$$
$$g_q = \left[\frac{(1 - ikr_q)(3\cos^2(\theta_q) - 1)}{r_q^3} + \frac{k^2 \sin^2(\theta_q)}{r_q} \right] \tag{3}$$

where $q = |i - j|$, $r_q = qd$ is the distance between particles i and j, d is the inter-particle spacing, $k = |k| = 2\pi n(\lambda)/\lambda$ is the wavenumber of the ambient medium and θ_q is the angle between the dipole moment vector (*i.e.*, the polarization of the incident field in the scalar case) and the displacement vector directed from j to i. We will consider the case of $\theta_q = \pi/2$, *i.e.*, where the polarization is perpendicular to the chain axis (transverse excitation). From eqn (1)–(3) a set of N linear equations can be obtained:

$$\hat{A}p = E_{app} \tag{4}$$

where $\hat{A}$ is the $N \times N$ interaction matrix, p is $N \times 1$ dipole moment vector of the different particles and E_{app} is $N \times 1$ vector of the applied electric field at each particle's location. The term A_{ij} of the matrix $\hat{A}$ accounts for the interaction of particles i and j for $i \neq j$ (according to eqn (3)), and for each particle's response to an external excitation for $i = j$ (according to eqn (1)):

$$A_{ij} = \begin{cases} \alpha_s^{-1} & \text{for } i = j \\ -G_{|i-j|} & \text{for } i \neq j \end{cases} \tag{5}$$

The particles' dipole moments can be obtained from the inverse matrix $\hat{B} \equiv \hat{A}^{-1}$:

$$p = \hat{B}E_{app} \tag{6}$$

Typically, the matrix $\hat{A}$ is numerically inverted to obtain $\hat{B}$ and p. This formalism is exact when the nanoparticles are sufficiently small to be described as perfect dipoles but have shown to yield accurate predictions even for larger nanoparticles.[1,45] However, this numerical method acts as a black box such that important aspects of the physical dynamics remain clandestine. While approximate iterative solu-

tions exist,[46–52] which may give some insight into the underlying physics, a closed-form solution for the problem is generally non-existent. In the following subsections, we first discuss the existing analytical solution for infinite chains, and then derive an approximate closed-form solution for finite chains.

A. Infinite chains

For infinite chains illuminated by a plane wave, all the nanoparticles are imposed with equal dipole moment amplitudes, and phase profile that is dictated by the angle of the incident light. Therefore, instead of relying on eqn (1) to solve the chain's response, where a numerical calculation is required to find $E_{\text{loc},i}$, it is possible to define the effective polarizability of a nanoparticle within the infinite chain:[1]

$$\alpha_{\text{eff}} = (\alpha_{\text{s}}^{-1} - S(k_{\parallel}))^{-1}, \tag{7}$$

and from that to calculate the dipole moments according to the applied field by $p_i = \alpha_{\text{eff}} E_{\text{app},i}$. The chain's incident-angle-dependent structural factor is defined as $S(k_{\parallel}) = \sum\limits_{q \neq 0} G_q \cdot e^{-ik_{\parallel} \cdot r_j}$

and $k_{\parallel} = k \sin(\theta)$ is the parallel component of the incident wave vector. Furthermore, according to quasi-momentum conservation considerations, the directions of diffraction from an infinite chain can be obtained by:

$$k_{\parallel} + G_m = k^{t/r}_{\parallel,m} \tag{8}$$

where $G_m = 2\pi m/d$ is a reciprocal lattice vector, m denotes the order of diffraction and $k^{t/r}_{\parallel,m}$ is the parallel component of the transmitted/reflected wave vector of order m. This equation, also known as the grating equation, is of general validity to periodic structures and is not restricted to nanoparticle chains. When a certain diffraction order radiates at a grazing angle to the surface, $i.e.$, $k^{t/r}_{\parallel,m} = \pm k$, the RA condition is satisfied:[53]

$$k_{\parallel} + G_m = \pm k \tag{9}$$

B. The derived model for finite chains

To derive an insightful analytical solution for p for finite chains, we develop a model in which we approximate $\hat{A}$ by a different matrix, $\hat{A}_{\text{Model}}$, which can be analytically inverted. To that end, we first describe the single reciprocal system by two non-reciprocal systems, as described in Fig. 1. Explicitly, we perform an LU decomposition to $\hat{A}$, such that:§

$$\hat{A} = \hat{L}\hat{U} \tag{10}$$

where $\hat{L}$ and $\hat{U}$ are lower and upper triangular matrices, respectively. Hence, the solution for p can be obtained by successively solving the two following systems:

$$\hat{L}p_{\text{aux}} = E_{\text{app}}$$
$$\hat{U}p = p_{\text{aux}} \tag{11}$$

---

§We note that this kind of LU decomposition, without permutations, always exists provided that all the leading submatrices of $\hat{A}$ have a non-zero determinant.[64]
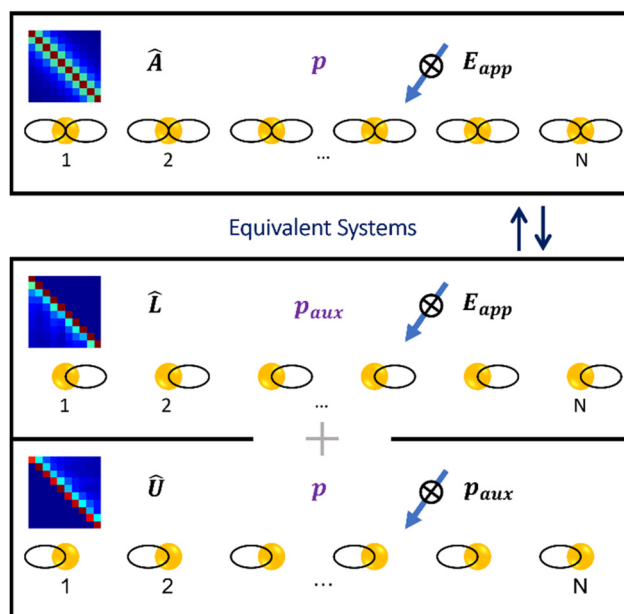
Fig. 1 The model's main simplification that enables obtaining an analytical solution. Decomposition of a single reciprocal system described by the interaction matrix $\hat{A}$, to two artificial non-reciprocal, one-way systems described by $\hat{L}$ and $\hat{U}$. The top figure depicts the reciprocal system according to $\hat{A}$, where the particles scatter symmetrically, and E_{app} is the applied field that serves to find p. The bottom figure shows the two non-reciprocal systems: first, excitation by E_{app} and asymmetric scattering to the right, according to $\hat{L}$, serves to find p_{aux}. Then, excitation by p_{aux} and asymmetric scattering to the left, according to $\hat{U}$, is used to find p. The black solid oblong patterns that emanate from each particle depict its associated radiation pattern. The polarization of the applied field is perpendicular to the chain axis, as marked in the illustration.

where the auxiliary dipole moment vector p_{aux}, which is obtained from the solution to the first set of equations, serves as the excitation for the second set. These two sets of equations correspond to two artificial non-reciprocal, one-way systems, which can be described by particles with asymmetrical scattering patterns. As can be seen in Fig. 1, the original system (top panel) is equivalent to superimposing the first system (middle panel), which is characterized by an interaction matrix $\hat{L}$ and has only scattering towards the right side of the chain (solid black oblongs lines emanating from the particles), to the second system (bottom panel), which is described by $\hat{U}$, and has only scattering towards the left side.

The derivation so far was exact. We proceed by taking advantage of the properties of $\hat{A}$ as a symmetrical Toeplitz matrix, $i.e.$, $A_{ij} = A_{i+1,j+1} = A_{|i-j|}$, and perform a simplifying approximation that, as we show, yields very accurate results. The fact that $\hat{A}$ is a symmetrical Toeplitz matrix is attributed to the interaction between the particles, which depends only on their distances, $i.e.$, $G(r_i - r_j) = G(|r_i - r_j|)$. We define a unit-less parameter that quantifies the strength of the nearest neighbor interaction, $\zeta \equiv g_1 \alpha_{\text{s}}$, where g_1 is defined in eqn (3). Then, for weakly interacting nearest neighbors, $i.e.$, for sufficiently small

$|\zeta|$, $\hat{L}$ and $\hat{U}$ can be expressed by elements of $\hat{A}$ (see Section 1 of the ESI† for an exact derivation of the validity condition). Specifically, if we decompose $\hat{A}$ to its lower and upper triangular parts as follows:

$$A_{ij}^L = \begin{cases} A_{ij} & \text{for } i \geq j \\ 0 & \text{for } i < j \end{cases}; \quad A_{ij}^U = (A_{ij}^L)^T \tag{12}$$

Then, we can approximate $\hat{L}$ and $\hat{U}$ to be:

$$\hat{L} \rightarrow \hat{L}_{\text{Model}} \equiv \sqrt{\alpha_s}\hat{A}^L \quad \hat{U} \rightarrow \hat{U}_{\text{Model}} \equiv \sqrt{\alpha_s}\hat{A}^U \tag{13}$$

By solving the original system, according to the two steps shown in Fig. 1 and with the model matrices $\hat{L}_{\text{Model}}$ and $\hat{U}_{\text{Model}}$, the solution for the particles' dipole moments can be found. Going through the described procedure is equivalent to solving the original system in eqn (4) with the model matrix $\hat{A}_{\text{Model}}$ instead of $\hat{A}$:

$$\hat{A} = \hat{L}\hat{U} \rightarrow \hat{A}_{\text{Model}} \equiv \alpha_s \hat{A}^L \hat{A}^U \tag{14}$$

The validation of the derived model by direct comparison of the exact numerical solution and the approximated analytical solution according to the model assumption in eqn (13) is presented in Section 2 of the ESI.†

In the following subsections, II-C and II-D, we present two different analytical solutions to the governing equation, eqn (6), according to the model in eqn (14), and discuss their unique physical interpretation. Namely, it is shown that while the two solutions are equivalent and describe the chain dynamics in terms of the same multi-scattering processes, the way in which these processes are counted differs in the two solutions and offers a different perspective for understanding the underlying interactions.

C. Solution based on a recursive interpretation

According to the above derivation, to solve for p we need to solve two systems with triangular Toeplitz matrices, each has an analytical solution for the required matrix inversion.[38,54] The inverse of $\hat{A}^L/\hat{A}^U$ is also a finite lower/upper triangular Toeplitz matrix:[54]

$$B_{ij}^L \equiv (A_{ij}^L)^{-1} = \begin{cases} B_{|i-j|} & \text{for } i \geq j \\ 0 & \text{for } i < j \end{cases} \tag{15}$$
$$B_{ij}^U = (B_{ij}^L)^T$$

where $B_q = B_{|i-j|}$ $(q = |i-j|)$ can be found based on the generalized Fibonacci polynomials:[54]

$$B_q = \alpha_s F_q^{(N-1)}(\vec{W}), \tag{16}$$

And $\vec{W} = (W_1, W_2, \dots, W_{N-1}) = \alpha_s(G_1, G_2, \dots, G_{N-1})$ is a weight vector that determines the contribution of each element in the recursive formula for $F_q^{(N-1)}(\vec{W})$:

$$F_q^{(N-1)}(\vec{W}) = \begin{cases} \sum_{i=1}^{N-1} W_i F_{q-i}^{(N-1)}(\vec{W}), & q > 0 \\ 1, & q = 0 \\ 0, & q < 0 \end{cases} \tag{17}$$

where $F_q^{(N-1)}(\vec{W})$ are the generalized Fibonacci polynomials. This recursive solution represents all possible multi-scattering paths between any two particles in the chain separated by exactly q unit cells, which may be regarded as the source and target of the scattering path. Specifically, B_q represents the effective response of the target particle to the applied field, such that the trivial response captured by α_s is modified to include all scattering paths in the chain originating from the source. Moreover, each of the B_q terms depends on all the previous B_i, *i.e.* $i < q$, such that only unidirectional scattering paths between the source and the target are considered.

To understand the multi-scattering perspective for the solution we first explain this interpretation for $q = 0$ and $q = 1$, and then consider higher q values for the general case. Afterwards, we implement this perspective on a specific case of four particles. For $q = 0$, eqn (16) and (17) give $B_0 = \alpha_s$, which describes only the trivial response of the particle to the applied field. For $q = 1$, $B_1 = \alpha_s(\alpha_s G_1)$ and describes the effective response of a target particle to the applied field in the presence of only one particle at a distance d, which acts as the source. This case for $q = 1$ is unique in the sense that only the source and target exist, such that in addition to the trivial response of the target to the applied field α_s, only the direct scattering from the source to the target $(\alpha_s G_1)$ is also included. For $q \geq 2$, B_q describes the effective response of the target particle in the presence of q preceding particles in the chain. The recursive relation includes the sum of q nonzero terms. Each term i ($i < q$) refers to an intermediate particle in the chain that precedes the target by exactly i unit cells. The intermediate particle defines a sub-chain of the total chain, which starts with the source particle and ends with the intermediate particle. First, the intermediate particle acts as a temporary target for the sub-chain such that the corresponding Fibonacci polynomial $F_{q-i}^{(N-1)}$ recursively includes all multi-scattering paths from the source to the intermediate particle. Next, the intermediate particle reemits light to the target of the chain as a direct scattering over i unit cells, disregarding all particles between the intermediate and target particles, represented by the corresponding weight term $W_i = \alpha_s G_i$. The sum over i defines the total recursive relation by alternatively assigning all q particles preceding the target as the intermediate particle. For the term $i = q$, the intermediate particle is the source such that only the direct scattering path over q unit cells is included.

To better understand the recursive interpretation, it is instructive to examine an example of a four-particle chain, as depicted in Fig. 2. According to eqn (16) and (17) we can find:

$$B_3 = B_0 \cdot \alpha_s G_3 + B_1 \cdot \alpha_s G_2 + B_2 \cdot \alpha_s G_1 \tag{18}$$

This describes the scattering, depicted in Fig. 2 (parentheses on the left), from particle 1 to particle 4 as follows: the first term defines particle 1 to be the intermediate particle and describes only the direct scattering from the first (B_0) to the fourth particle $(\alpha_s G_3)$. The second term defines particle 2 to be the intermediate particle and describes all the scattering paths from the first to the second particle (B_1) followed by the direct path from the second to the fourth particle $(\alpha_s G_2)$. The third

Counting Scattering Paths
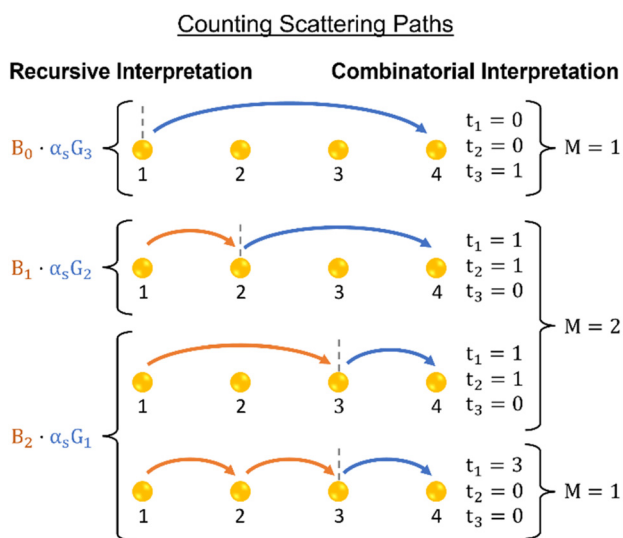
Fig. 2 Interpretation of the model's analytical solution in terms of multiple scattering process. The illustration depicts all scattering paths from particle 1 to particle 4, corresponding to B_3, while scattering only towards the right direction of the chain. The paths are counted according to the recursive interpretation on the left and according to the combinatorial interpretation on the right. The color of the arrows and the black dashed vertical lines correspond to the recursive interpretation. Left: The calculation relies on the division of the scattering from the first to the last particle into two segments. Explicitly, the first segment (orange) relies on the previously calculated B_q terms and corresponds to scattering over q particles, and the second segment (blue), which corresponds to $\alpha_s G_{N-1-q}$, accounts for the direct scattering over the remaining particles. For example, the top bracket depicts only the direct scattering from the first (B_0) to the fourth particle ($\alpha_s G_3$). The next bracket shows the scattering from the first to the second particle (B_1) and then the resulting path from the second to the fourth particle ($\alpha_s G_2$). The last bracket accounts for the two contributions of scattering from the first to the third particle (included in B_2) and then the resulting path from the third to the fourth particle ($\alpha_s G_3$). Right: The coefficients t_i's count how many hops of i particles exist in the path, and the multinomial coefficients, M's, count the degeneracy of the paths.

term defines particle 3 to be the intermediate particle and describes all the scattering paths from the first to the third particle (B_2) followed by the direct path from the third to the fourth particle ($\alpha_s G_1$).

To simplify the expression for B_q, we divide it to a complex amplitude term, b_q, and a phase term:

$$B_q = b_q e^{ikr_q} \tag{19}$$

The term e^{ikr_q} describes the phase accumulation of a wave propagating a distance of $r_q = qd$. By aiming to find b_q we can neglect the phase resulting from free-space propagation, which is especially beneficial around the RA condition. By substituting the relation $G_q = g_q e^{ikr_q}$ from eqn (3) into eqn (16), we note that the phase in each term of the recursive sum for B_q is e^{ikr_q}. Therefore, we find b_q to be:

$$b_q = \alpha_s F_q^{(N-1)}(\vec{w}) \tag{20}$$

where $\vec{w} = \alpha_s(g_1, g_2, \ldots, g_{N-1})$. We note that the calculations of B_q and b_q are much more efficient using the recursive relation in eqn (16)–(20), compared with the combinatorial solution presented in the next subsection, due to the ability to perform memoization. Explicitly, the calculation can be optimized by storing the results of previously calculated B_q and b_q and avoiding re-computation.

D. Solution based on a combinatorial interpretation

While the solution based on the generalized Fibonacci polynomials uncovers the recursive relations that are fundamental to the chain excitation, there is an additional important solution. This solution serves to explicitly count all multi-scattering paths between the source and target particles using a combinatorial interpretation and reveals essential properties of the multi-scattering processes that underly the particle interactions. The additional solution for B_q has the following form:[38]

$$B_q = \alpha_s \sum_{\vec{t} \in \mathbb{T}[q]} M(\vec{t}) \prod_{i=1}^{q} (\alpha_s G_i)^{t_i} \tag{21}$$

where $\vec{t}$ is a positive integer vector of length q with elements $t_1, \ldots, t_q$, and $\mathbb{T}[q]$ is a set of all vectors $\vec{t}$ that satisfy $\sum i t_i = q$, thereby specifying the summation condition. In addition, the multinomial coefficient is defined as:

$$M(\vec{t}) \equiv \binom{t_1 + \ldots + t_q}{t_1, \ldots, t_q} = \frac{(t_1 + \ldots + t_q)!}{t_1! t_2! \ldots t_q!} \tag{22}$$

In the following, we discuss the physical meaning of each of eqn (21) terms and show how it serves to count the multiple scattering paths in the chain. Specifically, we explain the physical meaning of the vector $\vec{t}$ and by looking at an example of a four-particle chain we show the source of the multinomial factor $M(\vec{t})$ in the equation.

Every vector $\vec{t}$ that obeys the summation condition represents a separate term of B_q, in which each component t_i ($1 \leq i \leq q$) of the vector appears as the exponent of $\alpha_s G_i$. This may be understood as the occurrence of t_i absorption-reemission processes of any two dipoles separated by i unit cells while maintaining the rule of a unidirectional scattering. Consequently, the total number of absorption-reemission processes in the term associated with each $\vec{t}$ is $T \equiv \sum_i t_i$, representing a multi-scattering path between two dipoles in the chain, i.e., the source and the target of the scattering path. For a general nonzero and not-restricted vector $\vec{t}$, this scattering path may include any number of absorption-reemission processes from one up to infinity and can describe a multi-scattering path between any two source and target dipoles in the chain. However, the components t_i of every vector $\vec{t}$ in the sum are limited by the summation condition, therefore defining which multi-scattering paths are permitted in addition to the distance between the source and the target of the scattering paths. Namely, each term $(\alpha_s G_i)^{t_i}$ in eqn (21) describes t_i absorption-reemission process over a total distance of $i t_i$ unit

cells. The summation condition $\sum i t_i = q$ therefore determines that only scattering paths over exactly q unit cells are included. Thus, B_q consists of all unidirectional multi-scattering paths between any two particles in the chain acting as a source and a target, where the two particles are separated by a distance qd.

To demonstrate the multi-scattering paths described by B_q in eqn (21) it is sufficient to look at a few small values of q. First, we see that $B_0 = \alpha_s$, which accounts for the particles' response to the applied field, and $B_1 = \alpha_s(\alpha_s G_1)$ describes the single direct scattering path that exists between nearest neighbors in the chain. For $q \geq 2$, the source and target of each multi-scattering path enclose at least one particle between them, such that on top of the direct scattering path over a distance of qd, all multi-scattering paths that include some or all the enclosed particles are added. For example, looking at the case of a four-particle chain, as shown in Fig. 2 (right parentheses), we see that there are four possible paths of scattering from particle 1 to particle 4. The first (top) path is the direct scattering path $1 \to 4$ over three unit cells, the second $1 \to 2 \to 4$ and third $1 \to 3 \to 4$ include only one of the particles 2 and 3, and describe scattering over one unit cell followed by scattering over two unit cells or *vice versa*, and the fourth path $1 \to 2 \to 3 \to 4$ includes all the particles between the source and the target and describes three consecutive scatterings over a distance of a unit cell each. The associated sum in B_3 has three terms corresponding to: first $t_1 = 0$, $t_2 = 0$, $t_3 = 1$, second $t_1 = 1$, $t_2 = 1$, $t_3 = 0$ and third $t_1 = 3$, $t_2 = 0$, $t_3 = 0$. The degeneracy of the two scattering paths $1 \to 2 \to 4$ and $1 \to 3 \to 4$, which both are described by $t_1 = 1$, $t_2 = 1$, $t_3 = 0$, is accounted for by the associated multinomial coefficient, $M = 2$, explaining its role in eqn (21). Generally, paths which are composed of similar scattering segments but ordered differently, correspond to a single term in the sum, with weight according to the associated multinomial coefficient. The number of scattering paths increases rapidly as a function of the number of particles (see Section 3 of the ESI†).

As we did in the recursive case, we can define combinatorically the b_q from eqn (21) by:

$$b_q = \alpha_s \sum_{\vec{t} \in \mathbb{T}[q]} M(\vec{t}) \prod_{i=1}^{q} (\alpha_s g_i)^{t_i} \tag{23}$$

Eqn (21) and (23) are equivalent to eqn (16) and (20), respectively. Specifically, the recursive sum in eqn (16) and (20) is replaced by an equivalent sum over the different scattering paths in eqn (21) and (23). Importantly, according to eqn (6), the solution for each p_q is determined by the elements of the matrix $\hat{B}$. Therefore, the underlying physical dynamics are embedded in the derived b_q terms.

To examine the appearance of nontrivial phase gradients over the chain and better understand the meaning of the B_q terms, it is insightful to examine the difference in the dipole moment of two adjacent particles in the chain. By considering first the solution of the unidirectional system described by $\hat{L}$, and for the case of normal incidence, *i.e.*, $E_{app,q} = E_0 (= 1 \text{ V nm}^{-1})$, we get:

$$\Delta p_{aux,q} \equiv p_{aux,q+1} - p_{aux,q} = B_q E^*_{app,q} \tag{24}$$

where $E^*_{app,q}$ denotes the complex conjugate of $E_{app,q}$. We see that B_q determines the difference in dipole moments of particles $q + 1$ and q. This result is expected since particle q experiences scattering from $q - 1$ particles from its left (particles 1 to $q - 1$), the same as particle $q + 1$ experiences scattering from $q - 1$ particles from its left (particles 2 to q). In addition, particle $q + 1$ experiences scattering from particle 1, described by B_q. We can generalize the relation in eqn (24) for the case of oblique incidence, $E_{app,q} = E_0 e^{-ik_\parallel r_q}$, by looking at the angle-normalized dipole-moment difference:

$$\Delta \tilde{p}_{aux,q} \equiv \tilde{p}_{aux,q+1} - \tilde{p}_{aux,q} = B_q E^*_{app,q} \tag{25}$$

where:

$$\tilde{p}_{aux,q} \equiv \frac{p_{aux,q}}{e^{i\phi_q}} \tag{26}$$

and $\phi_q = \arg(E_{app,q})$. By looking at $\tilde{p}_q$ and $\Delta \tilde{p}_q$ we eliminate the spatial phase profile in the chain attributed to the applied field and examine only the phase that arises due to the interaction between the nanoparticles. The second unidirectional system, described by $\hat{U}$, is solved in the same manner but for scattering in the opposite direction of the chain, according to Fig. 1. Thus, the equivalents of eqn (25) and (26) for that system are:

$$\Delta \tilde{p}_q \equiv \tilde{p}_{q+1} - \tilde{p}_q = -B_{N-q} p^*_{aux,q} \tag{27}$$

$$\tilde{p}_q \equiv \frac{p_q}{e^{i\phi_q}} \tag{28}$$

These quantities, *i.e.*, the angle-normalized dipole moment $\tilde{p}_q$ and its difference $\Delta \tilde{p}_q$, play an important role in the description of the excitation evolution along the chain. Specifically, in the vicinity of a RA condition, it is convenient to describe the difference in dipole moment from eqn (25) and (27), by the complex amplitude b_q. In particular, the insightful relations $\Delta \tilde{p}_{aux,q} \approx b_q$ or $\Delta \tilde{p}_q \approx -b_{N-q}$ hold near a RA towards the right side (positive order RA) or towards the left side (negative order RA) of the chain, respectively.

III. RA induced phase gradients

We apply the derived model to explore the emergence of phase gradients, defined with respect to the phase of the applied plane wave, that arise in finite chains at the vicinity of the RA condition for oblique incidence illumination. In what follows we show that at the RA condition the in-plane diffraction, which initiates at the chain edge, requires a finite length to build up. Therefore, before reaching this length, each particle contributes considerably to the formation of the diffraction, and consequently, the anomalous phase gradients are formed. We keep the discussion general by referring to the fundamental property that determines the optical response, *i.e.*, the polarizability, but we note that the values we analyze can be realized both with metallic and dielectric nanoparticles.[55] We examine the extreme cases of very small and very large

(maximal) polarizability, *i.e.*, off- and on-resonance, respectively, and the cases of on- and off-RA condition. For the on-resonance case, we consider the maximal magnitude of the polarizability at wavelength λ for a single mode, *i.e.*, the dipole mode in our case, which can be extracted from energy conservations considerations[55]

$$|\alpha_s^{Max}| = \frac{3}{2k^3} \quad (29)$$

This value is governed by the radiative loss and corresponds to the limit of negligible dissipative loss. We proceed by analyzing this limit, but note that even for varying dissipative rates up to the critical value where it equals the radiative loss rate, the reported effects of anomalous phase gradients and angular deviations persist (see Section IV for further discussion). Importantly, we note that even metals, in frequency ranges where they operate as good conductors, can possess negligible dissipative losses. For example, a gold nanorod of dimensions 190 nm × 100 nm × 100 nm supports the value of polarizability specified in eqn (29) for $\lambda = 1000$ nm (Section 4 of the ESI†). Based on this value of the polarizability at the resonance frequency, we examine the spectral response of a chain of identical nanoparticles with the following parameters: single nanoparticle polarizability with a Lorentzian[43,56,57] form of $\alpha_s = A_0(\omega_0^2 - \omega^2 + i\gamma\omega)$, amplitude $A_0 = 1 \times 10^{15}$ cm^3 s^{-2}, resonance angular frequency $\omega_0 = 2\pi c/\lambda_0$, resonance free-space wavelength $\lambda_0 = 1000$ nm, angular frequency $\omega = 2\pi c/\lambda$, where c is the speed of light, and damping constant $\gamma = 300$ Thz. A plot of the modeled polarizability is presented in Section 5 of the ESI.† In Fig. 3(a) we present the extinction cross section of a particle within an infinite chain, calculated according to:[58]

$$\sigma_{ext} = 4\pi k \cdot \Im(\alpha_{eff}) \quad (30)$$

where $\Im$ denotes the imaginary part, and α_{eff} is the effective polarizability defined in eqn (7). Fig. 3(a) shows σ_{ext} *vs.* wavelength and incident angle, for an infinite chain with the same parameters of the finite chain studied within the paper: ambient medium refractive index of $n = 1.5$, and an inter-particle spacing of $d = 420$ nm. The dashed white line corresponds to the $m = -1$ RA, plotted according to the momentum conservation condition in eqn (9).

The chain will be explored at the marked points in the figure: case A – off-resonance and off-RA ($\lambda = 1440$ nm, $\theta = 35.5°$) and case B – on-resonance and on-RA ($\lambda = 1000$ nm, $\theta = 35.5°$). In addition, in the ESI† we also numerically verify the model accuracy by examining case C – off-resonance and off-RA ($\lambda = 1440$ nm, $\theta = 0°$), and case D – on-resonance and off-RA ($\lambda = 1000$ nm, $\theta = 0°$).

To examine the emergence of anomalous phase gradients we now look at a finite chain with the same parameters of the infinite chain, at the vicinity of a unidirectional RA such that the inversion symmetry of the chain is broken. Specifically, we compare the chain dynamics of a 50-particle chain for a specific angle of incidence $\theta = 35.5°$, for cases A and B of Fig. 3(a). For that angle of incidence, we can find the wavelength of the $m = -1$ RA (coherent buildup from right to left)
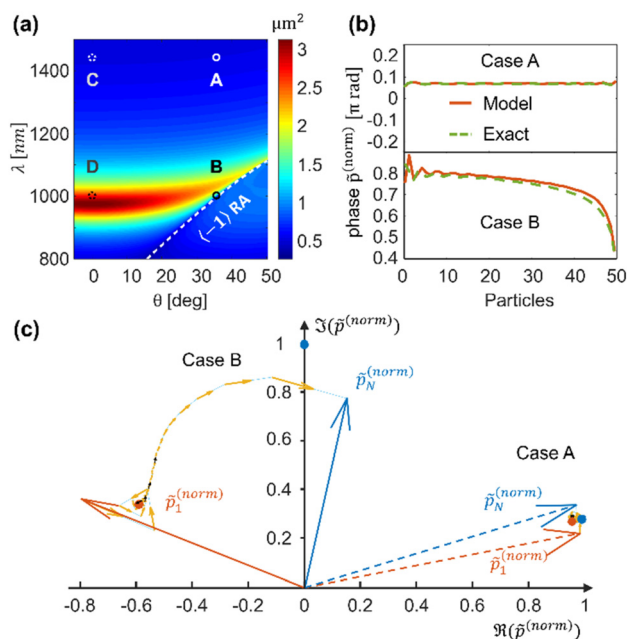
Fig. 3 RA induced phase gradients. (a) Optical extinction of an infinite chain with $d = 420$ nm and $n = 1.5$. These chain parameters are equivalent to the parameters of the finite chain studied within this paper. The dashed white line corresponds to the $\langle-1\rangle$ RA. (b) The phase of $\tilde{p}^{(norm)}$ as a function of the particle number for cases A and B in (a). The exact and model solution according to eqn (14), are presented. For case B, the nearly monotonic phase trend that spans ~0.5π rad can be seen. (c) The trajectory of $\tilde{p}_q^{(norm)}$ of all the particles in the chain, on the complex plane, for cases A (dashed lines) and B (solid lines). The orange arrows point to $\tilde{p}_1^{(norm)}$, and the blue arrows to $\tilde{p}_N^{(norm)}$. In the middle between these two, the yellow arrows, with the light blue guiding lines, show the difference in $\tilde{p}_q^N$. The arrows of every tenth particle are marked in black ($N = 10,20,30,40$). We note that the arrows for case B point to the direction of particles 1 to 50, while the coherent interaction, according to the $m = -1$ RA, is in the direction of particles 50 to 1. In addition, the blue and orange points show the excitation of the single particle, and the excitation of a particle within an infinite chain, respectively.

to be $\lambda = 996$ nm, using eqn (9). In Fig. 3(b) we examine the phase of the normalized dipole moment $\tilde{p}_q^{(norm)} = \tilde{p}_q/|p_s|$ of the chain's nanoparticles, for the two described cases. In the top part of Fig. 3(b), we show the case of off-resonance excitation and far from a RA (case A). We can see the minute oscillations of the phase, which spans less than 0.03π rad, and shows no monotonic trend. On the contrary, in the bottom part of Fig. 3(b), we excite the chain at the localized resonance of the nanoparticles and in vicinity to a RA (case B). We can see the nearly monotonic phase trend that spans ~0.5π rad. The phase gradually increases from the last to the first particle, according to the direction of the coherent scattering buildup for the $m = -1$ RA.

To better examine the chain excitation, in Fig. 3(c) we plot the trajectory of $\tilde{p}_q^{(norm)}$ of the nanoparticles in the chain, on the complex plane. The orange arrows point to $\tilde{p}_1^{(norm)}$, and the blue arrows to $\tilde{p}_N^{(norm)}$. In the middle, the yellow arrows with the light blue guiding lines show the consecutive differences

in $\tilde{p}_q^{(\text{norm})}$, such that the evolution of $\tilde{p}_q^{(\text{norm})}$ of the entire chain can be tracked. In addition, the blue points in the figure correspond to the excitation of the single nanoparticle:

$$p_{\text{s}}^{(\text{norm})} \equiv \frac{\alpha_{\text{s}}}{|\alpha_{\text{s}}|} = e^{i\phi_{\alpha_{\text{s}}}} \tag{31}$$

where $\phi_{\alpha_{\text{s}}} = \arg(\alpha_{\text{s}})$. This is equivalent to the excitation of a nanoparticle within a hypothetical chain with no interactions. The orange points in the figure correspond to the excitation of a nanoparticle within an infinite chain with the same parameters:[59]

$$p_{\infty}^{(\text{norm})} = \frac{\alpha_{\text{eff}}}{|\alpha_{\text{s}}|} \tag{32}$$

where α_{eff} is defined in eqn (7). In addition, to easily track the evolution of the chain as a function of the number of particles, we mark every 10 particles with a black arrow (particles 10,20,30,40 are marked).

We can see in Fig. 3(c) that the entire range of evolution on the complex plane for case A is confined to a substantially smaller region. Moreover, for case A, the orange and blue points are very close, such that no substantial change of the single particle response occurs due to the interaction. On the other hand, the same two points for case B are considerably separated. Intriguingly, in that case, we can see that the end of the chain responds like the single-particle case, while the beginning of the chain responds like an infinite chain. This behavior is attributed to the coherent buildup of the $m = -1$ RA. The last particle of the chain experiences only the incoherent scattering from the rest of the chain, which sums up to a minor change in its local field and, therefore in its excitation, relative to the single-particle case. Explicitly, the incoherent scattering translates to $p_{\text{aux},N} \approx E_{\text{app},N}$, which in turn translates to $p_N \approx \alpha_{\text{s}}E_{\text{app},N}$. Proceeding from that particle towards the beginning of the chain, each particle experiences a superposition of incoherent scattering from its left, and coherent scattering from its right. While the strength of the incoherent scattering does not change much from particle to particle, the coherent scattering changes significantly as more particles are added. This is the source of the monotonic trend of the trajectory (particles 50 to 30), as further explained in the following. At some point ($\sim$ particle 30), adding more particles to the coherent scattering does not influence much the resulting amplitude of the scattered field. From that point to the beginning of the chain starts the observed spiral with minor variations in the excitations. In the very first particles of the chain (particles 1 to 5) the variations are larger. This is due to the absence of enough particles to the left, which contribute to the incoherent scattering that each of these edge particles experiences. Namely, when only a small number of particles interfere incoherently, the resulting electric field is non negligible. Interestingly, the described behavior of the nanoparticle chain is the same for a larger number of inclusions (see Section 7 of the ESI†), where the anomalous phase evolution spans over $\sim$20 particles from the end of the chain.

IV. RA induced angular reflection anomaly

So far, we have investigated how the RA induces anomalous phase gradients of the particle's excitation. However, although these gradients can be probed by interferometric measurements,[60,61] their notable implication are the associated angular anomalies. Specifically, we show that the light reflected and diffracted from the chain deviates from the grating equation (eqn (8)) for infinite chains. Fig. 4(a) illustrates the phenomenon, where the incident light is diffracted at the RA anomaly condition at a grazing angle to the surface (order $m = -1$) and cause a deviation of the specular reflection by $\Delta\theta$ with respect to the infinite chain reflection. In Fig. 4(b) we compare the angular distribution of the specular reflection of a finite- and an infinite-chain with the same parameters, for two different wavelengths (cases A and B in Fig. 3(a)). The vertical orange lines show the expected direction of specular reflection for the infinite chain, *i.e.*, $\Delta\theta = 0$. We can see that for the off-resonance case, in the top figure, the reflected power is centered around $\Delta\theta = 0$. In contrast, for the on-resonance case, at the bottom, the reflection is shifted to $\Delta\theta = 0.23°$. This angular deviation occurs due to the phase gradient that spans $\sim$20 particles at the end of the chain, as discussed in Section III. Therefore, it is manifested in all the other diffraction orders as well. The direction of the observed shift is consistent with the slope of the phase gradient, and its magnitude is equal to 12.5% of the full width at half the maximum (FWHM) of the specular reflection. In Fig. 4(c) we show the angular deviation as a function of wavelength for chains of different lengths. The angular deviation peaks around the RA condition (black vertical line), whereas, as expected, the deviation is more pronounced for shorter chains. As the chain becomes longer the FWHM of the diffracted beams becomes smaller, therefore it is insightful to look at angular deflection normalized to the associated FWHM. In Fig. 4(d) we show the normalized $\Delta\theta$ at the wavelength of maximal deviation around the RA *vs.* the chain length (blue dots) and a fit to the function $a \cdot \exp(-N/b)$ (orange line). The extracted decay parameter is $b = 555$, which emphasizes the slow decay of the effect *vs.* the number of particles. Specifically, even to a 1000-particle chain (length of 420 microns), there is still a deviation of 2.5%. The decay of the effect for bigger chains can be understood as follows: the phase gradients span a constant number of particles ($\sim$20) at the edge of the chain. For any chain with more particles, the gradient will span predominantly these particles, while the rest of the chain will respond mostly like an infinite chain. The diffraction pattern can be regarded as emanating from the two parts of the chain: the first part, with the phase gradient, supports the angular deviation while the second part, with the infinite-like response, diffracts according to the grating equation. Therefore, as the chain gets larger, the contribution of the first part, which causes the angular deviation, to the total diffraction gets smaller, and the overall deviation decays. For typical experimentally explored arrays with lengths of 100
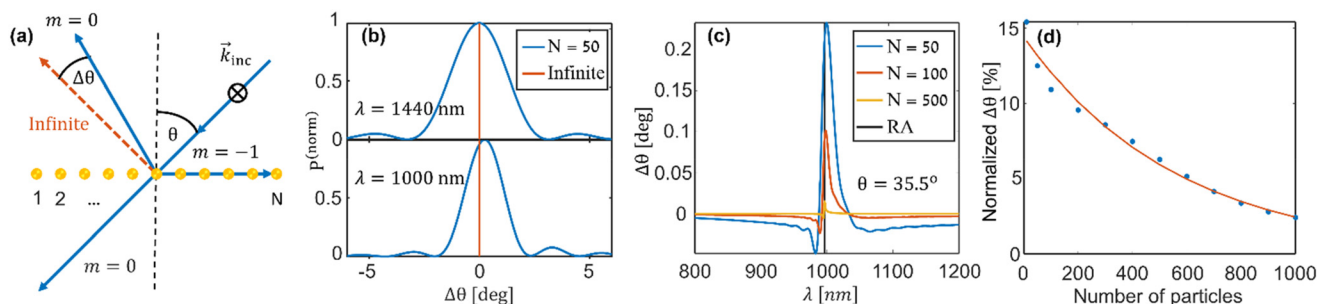
Fig. 4 Angular reflection anomaly. (a) Illustration of the finite chain illuminated at the RA condition. The grazing order $m = -1$ cause a deviation of the specular reflection by $\Delta\theta$ with respect to the infinite chain reflection. (b) The normalized power of the specular reflection for (top) off- and (bottom) on-resonance cases (cases A and B in Fig. 3(a)). The orange vertical lines show the direction of reflection for infinite chain, *i.e.*, $\Delta\theta = 0$. For the off-resonance case, the reflection is co-centered with the infinite chain reflection, while for the resonating particles at the RA condition, a shift of $\Delta\theta = 0.23°$ is seen. (c) The angular deviation as a function of wavelength for chains of different lengths. The angular deviation peaks around the RA condition (black vertical line), whereas the deviation is more pronounced for shorter chains. (d) The maximal angular deviation around the RA normalized to the associated FWHM of the reflected beam as a function of the chain length (blue dots), and a fit to the function $a \cdot \exp(-N/b)$ (orange line). The fit parameters are amplitude of $a = 0.14$ and decay length of $b = 555$, which emphasis the slow decay of the effect *vs.* the number of particles.

to 500 microns, the deviation would be 9% to 2% of the FWHM, correspondingly. We note that we focused on analyzing the reported effects of RA induced phase gradients and angular anomalies for the polarizability value specified in eqn (29), which corresponds to no dissipative loss, but these effects persist also for larger loss rates, even up to the critical value where the dissipative and the radiative loss rates are equal.[55] Specifically, for this critical coupling we found that for a 50-particle chain, the angular deviation with respect to the FWHM changes from 12.5% to 7.6% (see Section 12 of the ESI†).

V. Scattering path interference

The presented theoretical framework enables us to explore the buildup of the chain excitation as originating from interference of the multiple scattering paths. In Fig. 5, we show the scattering paths at the chain, and their interference with each other.¶ The figure presents the various terms that contribute to b_q, for the off- (Fig. 5(a) and (c), $\zeta = 0.05 \cdot e^{0.19i\pi}$) and on-(Fig. 5(b) and (d), $\zeta = 0.37 \cdot e^{0.58i\pi}$) resonance cases.

We note that B_q and b_q are intrinsic to the chain, and do not depend on the applied field parameters, nor on the number of particles in the chain. In Fig. 5(a) and (b) we show the terms contributing to b_3, and in Fig. 5(c) and (d), the terms contributing to b_{30}. In b_3 the interference is composed of three scattering paths, as shown in Fig. 2. The first yellow arrow corresponds to the $1 \rightarrow 2 \rightarrow 3 \rightarrow 4$ path, the second to the $1 \rightarrow 2 \rightarrow 4$ and $1 \rightarrow 3 \rightarrow 4$ paths, and the third to the $1 \rightarrow 4$ path. We note that the first arrow in Fig. 5(a) is vanishingly small. In the off-resonance case, the different terms add up almost coherently (*i.e.*, with the same phase), giving rise to a total b_q
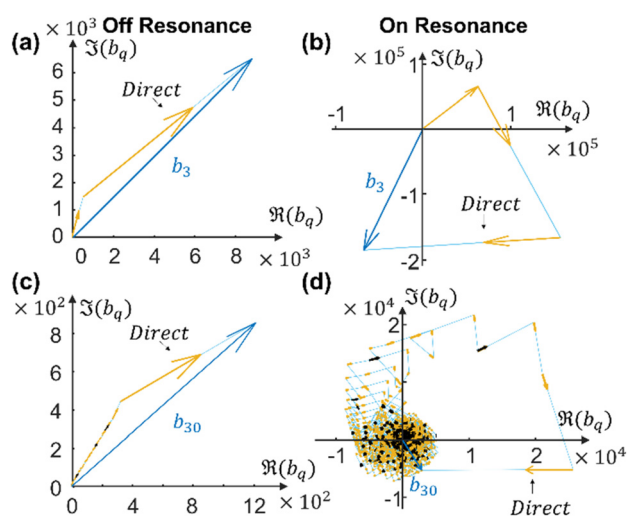
Fig. 5 Scattering path interference. The paths contributing to the complex amplitude b_q are shown for $q = 3$ in (a) and (b) and for $q = 30$ in (c) and (d). In addition, (a) and (c) correspond to the off-resonance case (1440 nm) while (b) and (d) to the on-resonance case (1000 nm). In (a) and (b) the interference is composed of three scattering paths, according to Fig. 2. We note that the first arrow in (a) is vanishingly small. In the off-resonance case, the different terms add up almost coherently (*i.e.*, with the same phase), giving rise to a total b_q that is considerably larger than each of the paths contributing to it. On the other hand, in the on-resonance case, the path interference is more complex, leading to the observed triangular shapes. This morphology takes place due to the resonant response of the nanoparticles, where the phase of α_s is imprinted and cascaded in the interference pattern. Specifically, the paths are ordered by the number of the absorption–remission processes they include (*i.e.*, according to $T \equiv \sum t_i$).[62] Therefore, paths with successive values of T have a nearly constant phase difference between them, which gives rise to the observed triangular shapes.

that is considerably larger than each of the paths contributing to it. On the other hand, in the on-resonance case, the path interference is more complex, as the relative angle between successive arrows is significantly larger than in Fig. 5(a). This

---

¶The computation of the partition of q for the different t_i according to $t_1 + 2t_2 + \ldots + qt_q = q$ (eqn (21)), was performed using.[62]

morphology takes place due to the resonant response of the nanoparticles, where the phase of α_s is imprinted and cascaded in the interference pattern. Specifically, the paths are ordered by the number of the absorption-remission processes they include (*i.e.*, according to $T \equiv \sum t_i$).[62] Therefore, paths with successive values of T have nearly constant phase differences between them, which gives rise to the observed triangular shapes. In Section 8 of the ESI,† we show how the mechanism that gives rise to the RA induced phase gradients can be understood from the dependence of b_q on q.

VI. Macroscopic description of the chain's dynamics

The theoretical point of view that was adopted in this paper considers the microscopic dynamics of the chain, *i.e.*, analyzes the excitation of each particle. Alternatively, the chain dynamics can be viewed by a macroscopic description, *via* the introduction of global wave functions that encapsulate the microscale interactions. In such analysis, the different wave phenomena can be discerned from the analytic properties of the chain's Green function.[25] Specifically, this approach reveals two distinct wave phenomena that are of dominant importance to finite or semi-finite chains with inter-particle spacing larger than $\lambda/2$: leaky modes and continuous spectrum waves. In this case, guided modes of any type, confined or light-cone, cannot be supported. Leaky modes can be found by searching the zeros of the chain's equation of dynamics, or equivalently, by seeking for the Poles of the chain's spectral Green function, and are characterized by an exponential decay of their amplitude along the chain. Conversely, the continuous spectrum waves are associated with branch-cut singularities of the chain's spectral Green's function and show an algebraic decay.[25] In Section 10 of the ESI,† we show that the phenomenon discussed in this paper, RA-induced phase gradients, is associated with the excitation of a continuous spectrum wave through a diffraction order of the impinging wave wavenumber. The interference between the specular reflection and the resonantly coupled continuous spectrum wave back to the wavenumber of the impinging wave results in the anomaly of the diffracted and reflected light.

VII. Conclusions

In this paper, we have developed a multiple scattering model to analyze the spatial excitation in finite nanoparticle chains. With this model, we demonstrated and analyzed a novel phenomenon of RA induced phase gradients in finite nanoparticle chains. These phase gradients are rooted in the finite length it takes for the in-plane diffraction at the RA condition to build up. The gradients are inherent to finite chains with resonant nanoparticles and in spectral vicinity to a unidirectional RA, *i.e.*, towards one direction of the chain. The induced phase profiles also affect the diffraction and specular reflection from the chain. Specifically, it causes a deviation of the diffraction pattern with respect to the infinite chain.

The analytical model treats the chain, a reciprocal system, by a successive solution of two non-reciprocal systems. Then, by approximating the governing matrices, we find a closed-form solution to the particle dipole moments. Intriguingly, the solution enables describing the excitation as originating from the interference of multiple scattering paths within the chain. Moreover, we show that the multiple scattering process can be accounted for by the generalized Fibonacci series, which reveals the recursive relation that underlies the chain excitation. Extension of the presented model to the case of two- and three-dimensional geometries may be trivial for the common case where the coherent interaction predominantly occurs in only one of the dimensions, and otherwise may require further formulation based on block matrix analysis. The model presented in this paper is important for analyzing finite arrays and the various phenomena that they can exhibit. Recently, the matured technology from the microwave regime of traveling-wave antenna, which relies on finite-size effects, is being investigated for miniaturized directive beam scanners in optical arrays.[23,24,63] We believe that the analysis of these systems, as well as general beam shaping schemes, can benefit from the developed framework, as it establishes a complementary microscopic picture to the well-established macroscopic theory of particle arrays. Moreover, the model may find use also in the description of finite disordered systems or other systems with weakly coupled components.

Conflicts of interest

There are no conflicts to declare.

Acknowledgements

References

1 V. G. Kravets, A. V. Kabashin, W. L. Barnes and A. N. Grigorenko, Plasmonic Surface Lattice Resonances: A Review of Properties and Applications, *Chem. Rev.*, 2018, 5912–5951, DOI: **10.1021/acs.chemrev.8b00243**.

2 W. Wang, M. Ramezani, A. I. Väkeväinen, P. Törmä, J. G. Rivas and T. W. Odom, The Rich Photonic World of Plasmonic Nanoparticle Arrays, *Mater. Today*, 2018, **21**(3), 303–314, DOI: **10.1016/J.MATTOD.2017.09.002**.

3 A. D. Utyushev, V. I. Zakomirnyi and I. L. Rasskazov, Collective Lattice Resonances: Plasmonics and Beyond, *Rev. Phys.*, 2021, **6**, 100051, DOI: **10.1016/j.revip.2021.100051**.

4 L. Michaeli, S. Keren-Zur, O. Avayu, H. Suchowski and T. Ellenbogen, Nonlinear Surface Lattice Resonance in Plasmonic Nanoparticle Arrays, *Phys. Rev. Lett.*, 2017, **118**(24), 243904, DOI: **10.1103/PhysRevLett.118.243904**.

5 O. Doron, L. Michaeli and T. Ellenbogen, Direct and Cascaded Collective Third-Harmonic Generation in Metasurfaces, *J. Opt. Soc. Am. B*, 2019, **36**(7), E71–E77, DOI: **10.1364/josab.36.000e71**.

6 R. Czaplicki, A. Kiviniemi, J. Laukkanen, J. Lehtolahti, M. Kuittinen and M. Kauranen, Surface Lattice Resonances in Second-Harmonic Generation from Metasurfaces, *Opt. Lett.*, 2016, **41**(12), 2684, DOI: **10.1364/OL.41.002684**.

7 S. Chen, B. Reineke, G. Li, T. Zentgraf and S. Zhang, Strong Nonlinear Optical Activity Induced by Lattice Surface Modes on Plasmonic Metasurface, *Nano Lett.*, 2019, **19**(9), 6278–6283, DOI: **10.1021/acs.nanolett.9b02417**.

8 R. Kolkowski, T. K. Hakala, A. Shevchenko and M. J. Huttunen, Nonlinear Nonlocal Metasurfaces, *Appl. Phys. Lett.*, 2023, **122**(16), 160502, DOI: **10.1063/5.0140483**.

9 L. Michaeli, H. Suchowski and T. Ellenbogen, Near–Infrared Tunable Surface Lattice Induced Transparency in a Plasmonic Metasurface, *Laser Photonics Rev.*, 2020, **14**(1), 1900204, DOI: **10.1002/lpor.201900204**.

10 S. R. K. Rodriguez, O. T. A. Janssen, G. Lozano, A. Omari, Z. Hens and J. G. Rivas, Near-Field Resonance at Far-Field-Induced Transparency in Diffractive Arrays of Plasmonic Nanorods, *Opt. Lett.*, 2013, **38**(8), 1238, DOI: **10.1364/ol.38.001238**.

11 M. Manjappa, Y. K. Srivastava and R. Singh, Lattice-Induced Transparency in Planar Metamaterials, *Phys. Rev. B*, 2016, **94**(16), 161103, DOI: **10.1103/PhysRevB.94.161103**.

12 B. D. Thackray, V. G. Kravets, F. Schedin, G. Auton, P. A. Thomas and A. N. Grigorenko, Narrow Collective Plasmon Resonances in Nanostructure Arrays Observed at Normal Light Incidence for Simplified Sensing in Asymmetric Air and Water Environments, *ACS Photonics*, 2014, **1**(11), 1116–1126, DOI: **10.1021/ph5002186**.

13 R. R. Gutha, S. M. Sadeghi, C. Sharp and W. J. Wing, Biological Sensing Using Hybridization Phase of Plasmonic Resonances with Photonic Lattice Modes in Arrays of Gold Nanoantennas, *Nanotechnology*, 2017, **28**(35), 355504, DOI: **10.1088/1361-6528/aa7bb5**.

14 A. A. Yanik, A. E. Cetin, M. Huang, A. Artar, S. H. Mousavi, A. Khanikaev, J. H. Connor, G. Shvets and H. Altug, Seeing Protein Monolayers with Naked Eye through Plasmonic Fano Resonances, *Proc. Natl. Acad. Sci. U. S. A.*, 2011, **108**(29), 11784–11789, DOI: **10.1073/pnas.1101910108**.

15 K.-H. Chang, J.-S. Cheng, T.-W. Lu and P.-T. Lee, Engineering Surface Lattice Resonance of Elliptical Gold Nanodisk Array for Enhanced Strain Sensing, *Opt. Express*, 2018, **26**(25), 33215–33225, DOI: **10.1364/oe.26.033215**.

16 W. Zhou, M. Dridi, J. Y. Suh, C. H. Kim, D. T. Co, M. R. Wasielewski, G. C. Schatz and T. W. Odom, Lasing Action in Strongly Coupled Plasmonic Nanocavity Arrays, *Nat. Nanotechnol.*, 2013, **8**, 506–511, DOI: **10.1038/nnano.2013.99**.

17 A. Yang, T. B. Hoang, M. Dridi, C. Deeb, M. H. Mikkelsen, G. C. Schatz and T. W. Odom, Real-Time Tunable Lasing from Plasmonic Nanocavity Arrays, *Nat. Commun.*, 2015, **6**(1), 6939, DOI: **10.1038/ncomms7939**.

18 T. K. Hakala, H. T. Rekola, A. I. Väkeväinen, J.-P. Martikainen, M. Nečada, A. J. Moilanen and P. Törmä, Lasing in Dark and Bright Modes of a Finite-Sized Plasmonic Lattice, *Nat. Commun.*, 2017, **8**, 13687, DOI: **10.1038/ncomms13687**.

19 D. Wang, A. Yang, W. Wang, Y. Hua, R. D. Schaller, G. C. Schatz and T. W. Odom, Band-Edge Engineering for Controlled Multi-Modal Nanolasing in Plasmonic Superlattices, *Nat. Nanotechnol.*, 2017, **12**(9), 889, DOI: **10.1038/nnano.2017.126**.

20 T. K. Hakala, A. J. Moilanen, A. I. Väkeväinen, R. Guo, J.-P. Martikainen, K. S. Daskalakis, H. T. Rekola, A. Julku and P. Törmä, Bose–Einstein Condensation in a Plasmonic Lattice, *Nat. Phys.*, 2018, **14**(7), 739–744, DOI: **10.1038/s41567-018-0109-9**.

21 R. E. Collin and F. J. Zucker, *Antenna Theory, Part 2*, McGraw-Hill, Inc., 1969.

22 D. R. Jackson, C. Caloz and T. Itoh, Leaky-Wave Antennas, in *Proceedings of the IEEE*, 2012. DOI: **10.1109/JPROC.2012.2187410**.

23 F. Monticone and A. Alù, Leaky-Wave Theory, Techniques, and Applications: From Microwaves to Visible Frequencies, *Proc. IEEE*, 2015, **103**(5), 793–821, DOI: **10.1109/JPROC.2015.2399419**.

24 D. R. Jackson, P. Burghignoli, G. Lovat, F. Capolino, J. Chen, D. R. Wilton and A. A. Oliner, The Fundamental Physics of Directive Beaming at Microwave and Optical Frequencies and the Role of Leaky Waves, *Proc. IEEE*, 2011, **99**(10), 1780–1805, DOI: **10.1109/JPROC.2010.2103530**.

25 Y. Hadad and B. Z. Steinberg, Green's Function Theory for Infinite and Semi-Infinite Particle Chains, *Phys. Rev. B: Condens. Matter Mater. Phys.*, 2011, **84**(12), 125402, DOI: **10.1103/PhysRevB.84.125402**.

26 Y. Hadad, Y. Mazor and B. Z. Steinberg, Green's Function Theory for One-Way Particle Chains, *Phys. Rev. B: Condens. Matter Mater. Phys.*, 2013, **87**(3), 035130, DOI: **10.1103/PhysRevB.87.035130**.

27 S. Campione, S. Steshenko and F. Capolino, Complex Bound and Leaky Modes in Chains of Plasmonic Nanospheres, *Opt. Express*, 2011, **19**(19), 18345–18363, DOI: **10.1364/oe.19.018345**.

28 J. P. Martikainen, A. J. Moilanen and P. Törmä, Coupled Dipole Approximation across the Γ-Point in a Finite-Sized Nanoparticle Array, in *Philosophical Transactions of the Royal Society A: Mathematical, Physical and Engineering Sciences*, 2017. DOI: **10.1098/rsta.2016.0316**.

29 D. Wang, M. R. Bourgeois, J. Guan, A. K. Fumani, G. C. Schatz and T. W. Odom, Lasing from Finite Plasmonic Nanoparticle Lattices, *ACS Photonics*, 2020, **7**(3), 630–636, DOI: **10.1021/acsphotonics.0c00231**.

30 A. S. Kostyukov, I. L. Rasskazov, V. S. Gerasimov, S. P. Polyutov, S. v. Karpov and A. E. Ershov, Multipolar Lattice Resonances in Plasmonic Finite-Size Metasurfaces, *Photonics*, 2021, **8**(4), 109, DOI: **10.3390/photonics8040109**.

31 L. Zundel, J. R. Deop-Ruano, R. Martinez-Herrero and A. Manjavacas, Lattice Resonances Excited by Finite-Width Light Beams, *ACS Omega*, 2022, **45**, 20, DOI: **10.1021/ACSOMEGA.2C03847**.

32 M. A. Gorlach, X. Ni, D. A. Smirnova, D. Korobkin, D. Zhirihin, A. P. Slobozhanyuk, P. A. Belov, A. Alù and A. B. Khanikaev, Far-Field Probing of Leaky Topological States in All-Dielectric Metasurfaces, *Nat. Commun.*, 2018, **9**(1), 909, DOI: **10.1038/s41467-018-03330-9**.

33 D. Leykam and D. A. Smirnova, Probing Bulk Topological Invariants Using Leaky Photonic Lattices, *Nat. Phys.*, 2021, **17**, 632, DOI: **10.1038/s41567-020-01144-5**.

34 V. A. Fedotov, N. Papasimakis, E. Plum, A. Bitzer, M. Walther, P. Kuo, D. P. Tsai and N. I. Zheludev, Spectral Collapse in Ensembles of Metamolecules, *Phys. Rev. Lett.*, 2010, **104**(22), 223901, DOI: **10.1103/PhysRevLett.104.223901**.

35 D. M. Natarov, V. O. Byelobrov, R. Sauleau, T. M. Benson and A. I. Nosich, Periodicity-Induced Effects in the Scattering and Absorption of Light by Infinite and Finite Gratings of Circular Silver Nanowires, *Opt. Express*, 2011, **19**(22), 22176, DOI: **10.1364/OE.19.022176**.

36 S. R. K. Rodriguez, M. C. Schaafsma, A. Berrier and J. Gómez Rivas, Collective Resonances in Plasmonic Crystals: Size Matters, *Phys. B*, 2012, **407**(20), 4081–4085, DOI: **10.1016/j.physb.2012.03.053**.

37 L. Zundel and A. Manjavacas, Finite-Size Effects on Periodic Arrays of Nanostructures, *J. Phys.: Photonics*, 2018, **1**(1), 015004, DOI: **10.1088/2515-7647/aae8a2**.

38 M. Merca, A Generalization of the Symmetry between Complete and Elementary Symmetric Functions, *Indian J. Pure Appl. Math.*, 2014, **45**, 75, DOI: **10.1007/s13226-014-0052-0**.

39 V. Karimi and V. E. Babicheva, Dipole-Lattice Nanoparticle Resonances in Finite Arrays, *Opt. Express*, 2023, **31**(10), 16857, DOI: **10.1364/OE.491334**.

40 A. Alù and N. Engheta, Theory of Linear Chains of Metamaterial/Plasmonic Particles as Subdiffraction Optical Nanotransmission Lines, *Phys. Rev. B: Condens. Matter Mater. Phys.*, 2006, **74**(20), 205436, DOI: **10.1103/PhysRevB.74.205436**.

41 B. Z. Steinberg and Y. Hadad, One Way Optical Waveguides for Matched Non-Reciprocal Nanoantennas with Dynamic Beam Scanning Functionality, *Opt. Express*, 2013, **21**(101), A77–A83, DOI: **10.1364/OE.21.000A77**.

42 K. Lance Kelly, C. Eduardo, L. Z. Lin and G. C. Schatz, The Optical Properties of Metal Nanoparticles: The Influence of Size, Shape, and Dielectric Environment, 2002. DOI: **10.1021/JP026731Y**.

43 R. Kolkowski and A. F. Koenderink, Lattice Resonances in Optical Metasurfaces With Gain and Loss, *Proc. IEEE*, 2020, **108**(5), 795–818, DOI: **10.1109/JPROC.2019.2939396**.

44 B. Auguié and W. L. Barnes, Collective Resonances in Gold Nanoparticle Arrays, *Phys. Rev. Lett.*, 2008, **101**(14), 143902, DOI: **10.1103/PhysRevLett.101.143902**.

45 T. Jensen, L. Kelly, A. Lazarides and G. C. Schatz, Electrodynamics of Noble Metal Nanoparticles and Nanoparticle Clusters, *J. Cluster Sci.*, 1999, **10**(2), 295–317, DOI: **10.1023/A:1021977613319**.

46 R. Esteban, R. Vogelgesang, J. Dorfmüller, A. Dmitriev, C. Rockstuhl, C. Etrich and K. Kern, Direct Near-Field Optical Imaging of Higher Order Plasmonic Resonances, *Nano Lett.*, 2008, **8**(10), 3155–3159, DOI: **10.1021/nl801396r**.

47 D. N. Chigrin, C. Kremers and S. V. Zhukovsky, Plasmonic Nanoparticle Monomers and Dimers: From Nanoantennas to Chiral Metamaterials, *Appl. Phys. B*, 2011, **105**(1), 81–97, DOI: **10.1007/S00340-011-4733-7**.

48 L. Alekseyev, E. Narimanov and J. Khurgin, Super-Resolution Spatial Frequency Differentiation of Nanoscale Particles with a Vibrating Nanograting, *Appl. Phys. Lett.*, 2012, **100**(1), 11101, DOI: **10.1063/1.3673470**.

49 S. M. Hein and H. Giessen, Retardation-Induced Phase Singularities in Coupled Plasmonic Oscillators, *Phys. Rev. B: Condens. Matter Mater. Phys.*, 2015, **91**, 205402, DOI: **10.1103/PhysRevB.91.205402**.

50 N. Ustimenko, K. Baryshnikova, D. Kornovan, M. Beliakov and A. B. Evlyukhin, Born Series Using for Designing of All-Dielectric Metalenses, *AIP Conf. Proc.*, 2020, **2300**(1), 20007, DOI: **10.1063/5.0031976**.

51 N. Ustimenko, K. V. Baryshnikova, K. V. Baryshnikova, R. Melnikov, D. Kornovan, V. Ulyantsev, B. N. Chichkov, B. N. Chichkov, B. N. Chichkov, A. B. Evlyukhin, A. B. Evlyukhin and A. B. Evlyukhin, Multipole Optimization of Light Focusing by Silicon Nanosphere Structures, *J. Opt. Soc. Am. B*, 2021, **38**(10), 3009–3019, DOI: **10.1364/JOSAB.436139**.

52 N. A. Ustimenko, D. F. Kornovan, K. V. Baryshnikova, A. B. Evlyukhin and M. I. Petrov, Multipole Born Series Approach to Light Scattering by Mie-Resonant Nanoparticle Structures, *J. Opt.*, 2022, **24**(3), 035603, DOI: **10.1088/2040-8986/AC4A21**.

53 L. Rayleigh, On the Dynamical Theory of Gratings, *Proc. R. Soc. A*, 1907, **79**(532), 399–416, DOI: **10.1098/rspa.1907.0051**.

54 A. Sahin, Inverse and Factorization of Triangular Toeplitz Matrices, *Miskolc Math. Notes*, 2018, **19**(1), 527, DOI: **10.18514/mmn.2018.1780**.

55 S. Tretyakov, Maximizing Absorption and Scattering by Dipole Particles, *Plasmonics*, 2014, **9**(4), 935–944, DOI: **10.1007/s11468-014-9699-y**.

56 S. Zou and G. C. Schatz, Narrow Plasmonic/Photonic Extinction and Scattering Line Shapes for One and Two

Dimensional Silver Nanoparticle Arrays, *J. Chem. Phys.*, 2004, **121**(24), 12606–12612, DOI: **10.1063/1.1826036**.

57 S. Zou, N. Janel and G. C. Schatz, Silver Nanoparticle Array Structures That Produce Remarkably Narrow Plasmon Lineshapes, *J. Chem. Phys.*, 2004, **120**(23), 10871–10875, DOI: **10.1063/1.1760740**.

58 E. Hao, S. Li, R. C. Bailey, S. Zou, G. C. Schatz and J. T. Hupp, Optical Properties of Metal Nanoshells, *J. Phys. Chem. B*, 2004, **108**(4), 1224–1229, DOI: **10.1021/jp036301n**.

59 F. J. García de Abajo, Colloquium: Light Scattering by Particle and Hole Arrays, *Rev. Mod. Phys.*, 2007, **79**(4), 1267–1290, DOI: **10.1103/RevModPhys.79.1267**.

60 S. D. Gennaro, Y. Sonnefraud, N. Verellen, P. Van Dorpe, V. V. Moshchalkov, S. A. Maier and R. F. Oulton, Spectral Interferometric Microscopy Reveals Absorption by Individual Optical Nanoantennas from Extinction Phase, *Nat. Commun.*, 2014, **5**(1), 3748, DOI: **10.1038/ncomms4748**.

61 L. Michaeli, D. Ben Haim, M. Sharma, H. Suchowski and T. Ellenbogen, Spectral Interferometric Microscopy for Fast and Broadband Phase Characterization, *Adv. Opt. Mater.*, 2020, **8**(16), 2000326, DOI: **10.1002/adom.202000326**.

62 J. D'Errico, *Partition of an interger*. MATLAB Central File Exchange. **https://www.mathworks.com/matlabcentral/fileexchange/12009-partitions-of-an-integer**.

63 E. Abdo-Sanchez, M. Chen, A. Epstein and G. V. Eleftheriades, A Leaky-Wave Antenna with Controlled Radiation Using a Bianisotropic Huygens' Metasurface, *IEEE Trans. Antennas Propag.*, 2018, **67**(1), 108–120, DOI: **10.1109/TAP.2018.2878082**.

64 R. A. Horn and C. R. Johnson, *Matrix Analysis*, Cambridge University Press, 1985. DOI: **10.1017/CBO9780511810817**.